Journal of Applied Polymer Science

Strain-induced crystallization behavior of phenolic resin crosslinked natural rubber/clay nanocomposites

Abdulhakim Masa,[1] Sougo Iimori,[2] Ryota Saito,[2] Hiromu Saito,[2] Tadamoto Sakai,[3] Azizon Kaesaman,[1] Natinee Lopattananon[1]

[1]Department of Rubber Technology and Polymer Science, Faculty of Science and Technology, Prince of Songkla University, Pattani 94000, Thailand

[2]Department of Organic & Polymer Materials Chemistry, Tokyo University of Agriculture and Technology, Koganei-shi, Tokyo 184-8588, Japan

[3]Shizuoka University, 3-3-6 Shibaura, Minato, Tokyo 108-0023, Japan

Correspondence to: N. Lopattananon (E-mail: natinee.l@psu.ac.th)

ABSTRACT: Nanocomposites of natural rubber (NR) and unmodified clay were prepared by latex compounding method. Phenolic resin (PhOH) was used to crosslink NR. Crosslinked neat NR was also prepared for comparison. The structure–property relationship of uncrosslinked and crosslinked NR/clay nanocomposites was examined to verify the reinforcement mechanism. Microstructure of NR/clay nanocomposites was studied by using transmission electron microscopic (TEM), X-ray diffraction (XRD), wide angle X-ray diffraction (WAXD), and small angle X-ray scattering (SAXS) analyses. The results showed the evidence of intercalated clay together with clay tactoids for the nanocomposite samples. The highest tensile strength was achieved for the crosslinked NR/clay nanocomposite. The onset strain of deformation induced the crystallization of NR for nanocomposites was found at almost the same strain, and furthermore their crystallization was developed at lower strain than that of the crosslinked neat NR because of the clay orientation and alignment. However, at high strain region, the collaborative crystallization process related to the clay dispersion and conventional crosslink points in the NR was responsible to considerably high tensile strength of the crosslinked NR/clay nanocomposite. Based on these analyses, a mechanistic model for the strain-induced crystallization and orientational evolution of a network structure of PhOH-crosslinked NR/clay nanocomposite was proposed. © 2015 Wiley Periodicals, Inc. J. Appl. Polym. Sci. **2015**, *132*, 42580.

KEYWORDS: crystallization; composites; morphology; rubber; X-ray

Received 25 March 2015; accepted 3 June 2015

DOI: 10.1002/app.42580

INTRODUCTION

Natural rubber (NR) has been considered as an excellent renewable commodity material, which is used extensively for a wide range of products such as tires and conveyor belts.[1–3] Because NR has high structural regularity, it can exhibit strain-induced crystallization when stretching due to the ability of molecular chain arrangement along the stretching direction.[1–5] Owing to the strain-induced crystallization, NR can provide high tensile strength and resistance to cutting, tearing, and abrasion. Hence, the strain-induced crystallization is a significant subject to understand the characteristic properties of NR. The strain-induced crystallization mechanism of NR has been explained on the basis of inhomogeneous distribution of the network chain length, i.e., highly crosslinked network region, which would contribute to the molecular chain orientation to induce the crystallization.[4–7]

Today polymer nanocomposites reinforced by nanoclay have become of importance in polymer research fields and the industry because they exhibited outstanding properties over those of conventional neat polymers and filled ones.[8–13] For NR-based nanocomposites crosslinked with sulfur and peroxide, it was reported that the properties of NR crosslinked with sulfur and peroxide crosslinking agents such as modulus and tensile strength were significantly enhanced, if the clay was finely dispersed in the NR matrix. The property increase of crosslinked NR was attributed to microstructural change and clay mobility in a chemical network of NR.[14–20] This caused a decrease of strain for the onset of crystallization and the enhancement of crystallization. A strain-induced crystallization mechanism of crosslinked NR in the presence of nanoclay was proposed.[18] When the clay was dispersed in the crosslinked NR matrix, the clay was oriented and aligned during the elongation at low level of strain (<300%). This led to a decrease in onset

crystallization, subsequently the completely aligned clay along the stretching direction and to form physical network for the alignment of NR chain and the crystallization increased.[18] However, the role of clay in strain-induced crystallization of crosslinked NR was not clearly clarified in the past reports due to a morphological change of NR nanocomposites by the presence of crosslinked network. To clearly understand the property enhancement related to the morphological change of NR with clay and crosslink point, it is necessary to investigate the addition effect of clay on the crystallization behavior of uncrosslinked NR. So far, the strain-induced crystallization of uncrosslinked NR/clay has never been studied.

In this study, we prepared NR/clay nanocomposites by using unmodified (pristine) clay (abbr. clay). The NR/clay nanocomposites were obtained by a latex-compounding method due to the latex compounding has unique advantages of excellent dispersion of clay and less molecular weight reduction.[21] In addition, this method is promising for industrialization because of low cost of pristine clay, simplicity of preparation process and superior cost/performance ratio.[22,23] The phenolic crosslinking agent (abbr. PhOH) was used to cure the NR because it provides NR vulcanizates with more homogenous cross-links,[24] better heat resistance, lower compression set, better dynamic properties and optimum heat resistance/cost balance,[25–27] when the other crosslinking agents such as sulfur and peroxide are compared.

To our best knowledge, the strain-induced crystallization of PhOH-crosslinked NR/clay nanocomposites has also never been reported. To differentiate the effect of clay and conventional crosslinking on the strain-induced crystallization of NR, the mechanical properties and strain-induced crystallization of uncrosslinked and crosslinked NR nanocomposites were investigated by tensile test, wide angle X-ray diffraction (WAXD), and small angle X-ray scattering (SAXS). The clay dispersion was examined by using X-ray diffraction (XRD) analysis and transmission electron microscopy (TEM). Finally, a mechanistic model for reinforcement of PhOH-crosslinked NR/clay nanocomposite under the presence of nanoclay was proposed.

EXPERIMENTAL

Materials

NR latex consisting of dry rubber content of 60% and stabilized with high concentration of ammonium was supplied by Yala Latex Co. (Yala, Thailand). Unmodified clay, sodium montmorillonite (Na-MMT, Kunipia-F®), was kindly provided by Kunimine Industries Co. (Tokyo, Japan). Hydroxymethylol phenolic resin (HRJ-10518), having softening point of 80–95°C and a specific gravity of 1.05 was manufactured by Schenectady International (New York, USA) and used as crosslinking agent. Stannous chloride ($SnCl_2{\cdot}2H_2O$), with melting point and density of 37°C and 2.71 g/cm^3, manufactured by Carlo Erba Reagent (Val de Reuil, France) was used as catalyst for the crosslinking reaction of phenolic resin.

Preparation of NR/Clay Nanocomposites

Suspension of clay in water (2 wt %) was added into the NR latex to obtain uncrosslinked NR/clay nanocomposites. The

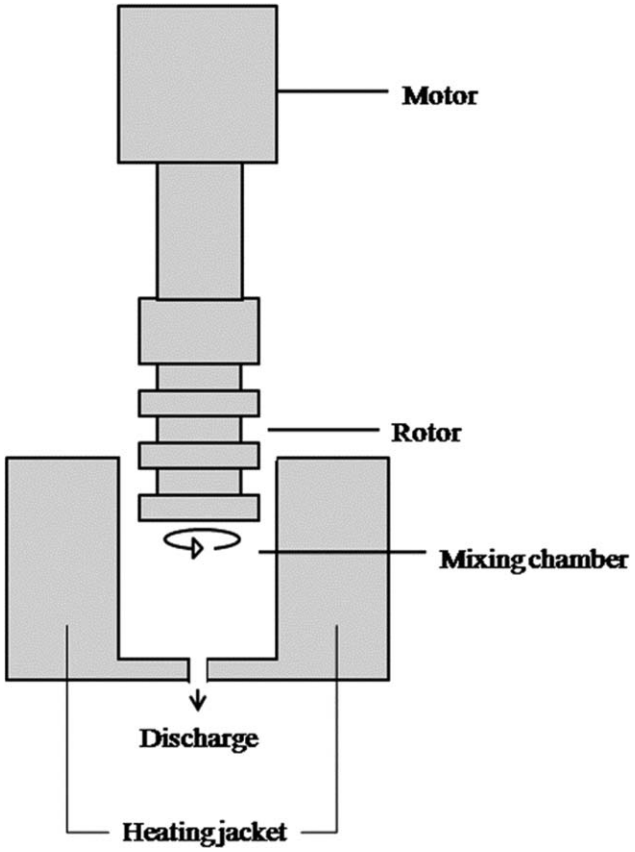

Figure 1. Schematic representation of a miniature mixing machine.

NR/clay mixture was firstly mixed under vigorous stirring (600 rpm) at ambient temperature for 30 min, and dried at 50°C for 3 days. For the preparation of PhOH-crosslinked NR nanocomposites, the NR/clay nanocomposite was compounded with a crosslinking agent (PhOH) and catalyst ($SnCl_2{\cdot}2H_2O$) in a mixing chamber of a miniature mixing machine (Figure 1) (IMC-18D7, Imoto Machinery Co., Japan) at rotor speed of 140 rpm and temperature of 100°C for 20 min. The sample was then melt pressed in a small hot-press machine (Imoto Machinery Co., Japan) at 180°C for 10 min to obtain the film with a thickness of 1 mm. The formulation of PhOH-crosslinked NR/clay nanocomposite is shown in Table I. The uncrosslinked and PhOH-crosslinked NR specimens without clay were also prepared by using the same procedure outlined above for the preparation of the uncrosslinked and PhOH-crosslinked NR nanocomposites, respectively.

Table I. Formulation of Phenolic Resin Crosslinked NR/Clay Nanocomposite

Ingredients	Part per hundred parts of rubber (phr)
NR	100
Clay (Na-MMT)	0 and 5
HRJ-10518 (phenolic resin)	10
$SnCl_2{\cdot}2H_2O$ (catalyst)	1

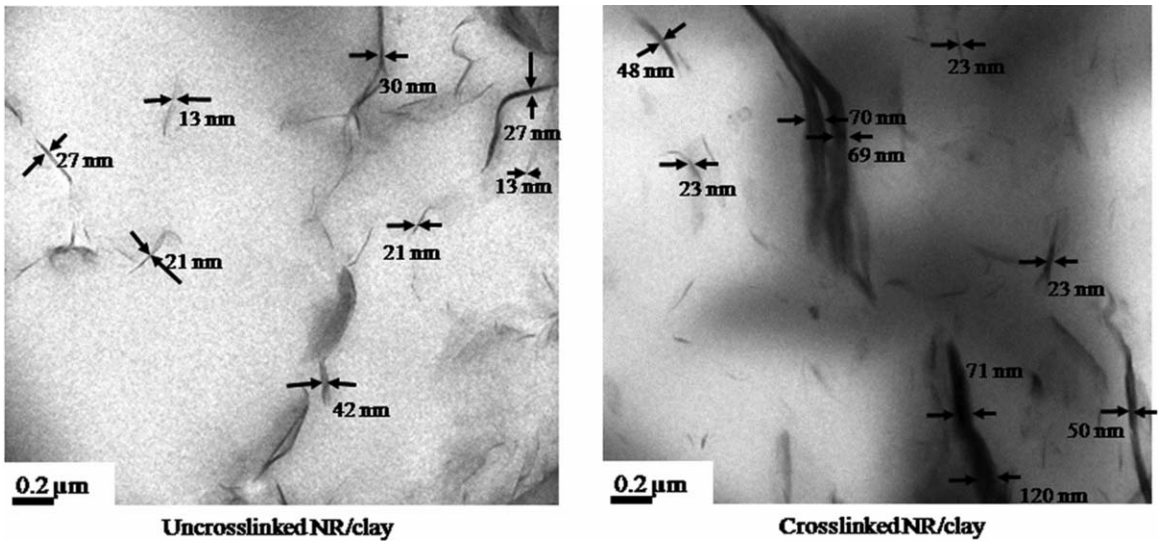

Figure 2. TEM images for uncrosslinked and phenolic resin-crosslinked NR/clay nanocomposites.

Characterizations

X-ray diffraction (XRD) (Rigaku TTRAXII, Japan) analysis was performed to measure the interlayer spacing (d_{001}) of pure clay and NR/clay nanocomposites. The X-ray beam was CuKα ($\lambda = 0.154$ nm) with voltage of 50 kV and current of 300 mA. Data were obtained at a scanning rate of 0.02°/min.

For the tensile test, the NR specimen was cut into a dumb-bell shape of 35 mm length. The stress–strain curve of the film specimen was obtained by using a tensile testing machine (StrographVES05D, Toyoseiki Co., Japan) at a crosshead rate of 300 mm/min at room temperature, according to JIS-K6251 and five specimens were used for the tensile test.

Transmission electron microscope (TEM) observation was performed to estimate the dispersion of clay in the nanocomposite samples. Ultra-thin sections about 100 nm in thickness were cut at −100°C using an ultra-cryomicrotome (Leica EM FC7). The sectioned samples were observed by using JEM-2100TEM (JEOL Co., Japan) at accelerating voltage of 200 kV.

Wide angle X-ray diffraction (WAXD) and small angle X-ray scattering (SAXS) measurements during stretching were performed by using NANO-Viewer system (Rigaku Co., Japan). A Cu-Kα radiation (46 kV, 60 mA) was generated and collimated by a confocal max-flux mirror system. The wavelength was 0.154 nm. The sample to detector distance was 15 mm for WAXD and 700 mm for SAXS, respectively. An imaging plate (IP) (Fujifilm BAS-SR 127) was used as a two-dimensional detector and the IP reading device (R-AXIS Ds3, Rigaku Co., Japan) was used to transform the obtained image to the text data. The sample was stretched in steps after WAXD or SAXS measurement at the fixed strain using a miniature tensile machine (Imoto Machinery Co., Japan). The exposure time was 15 min for WAXD and 1 h for SAXS measurements. All measurements were performed at room temperature (20°C). The scattering intensity was corrected with respect to the exposure time, the sample thickness, and the transmittance.

RESULTS AND DISCUSSION

Clay Dispersion

Figure 2 shows the TEM images of uncrosslinked and PhOH-crosslinked NR nanocomposites containing 5 phr clay. The dark lines are the intersections of the silicate layers (clay platelets). It is seen that the silicate layers were not exfoliated into single platelet, but they were intercalated by the rubber chain. It is also seen that the clay was not homogenously dispersed in the NR matrix and that the intercalated clay together with the nanometer sized aggregates of clay or tactoids were observed. The size of the clay tactoids were in the range of 10–50 nm and 12–120 nm in thickness in the uncrosslinked and crosslinked NR/clay, respectively, suggesting that the clay layers were stacked. The state of clay dispersion, i.e., the size of clay tactoids dispersed in the NR matrix, was changed after the crosslinking process with PhOH crosslinking agent. The reason for this change needs to be further investigated.

To confirm the microstructure of NR/clay nanocomposites, the XRD analysis was performed. Figure 3 shows the XRD patterns of pristine clay (Na-MMT), uncrosslinked and PhOH crosslinked NR nanocomposites filled with 5 phr clay. It is seen that the XRD pattern of pure nanoclay has a strong diffraction peak at $2\theta = 7.04°$, corresponding to interlayer spacing (d_{001}) between silicate platelets of 1.26 nm. The XRD pattern of NR nanocomposites showed two diffraction peaks at $2\theta = 3.44°$ and 6.26° for uncrosslinked sample and at $2\theta = 3.76°$ and 6.50° for crosslinked NR, corresponding to interlayer spacing of 2.57 and 1.41 nm and 2.35 and 1.36 nm, respectively. The decrease of intensity and broadening of the diffraction peaks at lower angle regions for the uncrosslinked and crosslinked NR/clay nanocomposites when compared with the diffraction peak of the pristine clay indicated that the rubber chains moved in between the gallery spacing of clay platelets, suggesting intercalated clay structure.[12] Based on the TEM and XRD results, the nanocomposites of NR and clay with intercalated clay structure and thin tactoids of nanometer scale could be confirmed.

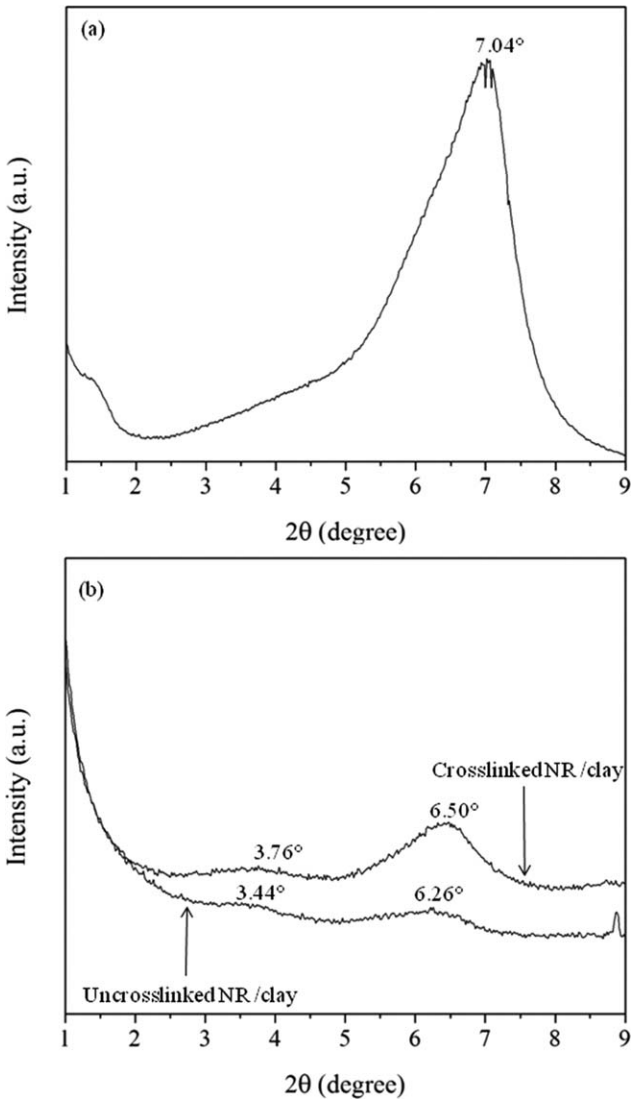

Figure 3. XRD patterns of (a) pristine clay and (b) NR/clay nanocomposites.

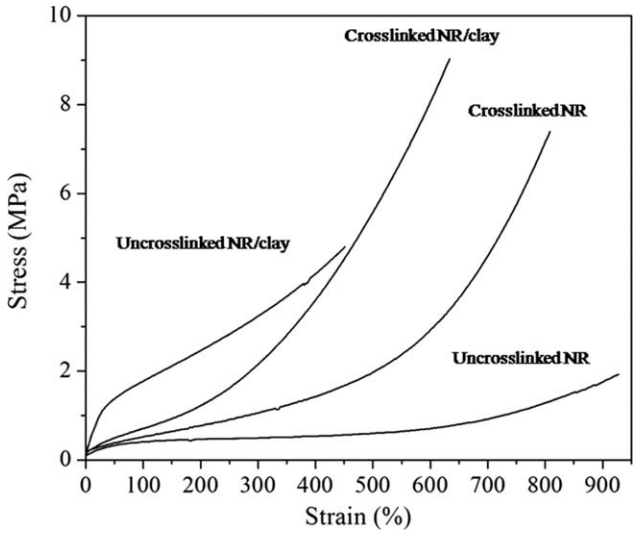

Figure 4. Stress–strain curves for uncrosslinked and phenolic resin-crosslinked NR with and without clay addition.

Stress-Strain Behavior

Figure 4 shows the stress–strain curves of the uncrosslinked and PhOH-crosslinked NR/clay nanocomposites. The stress–strain curves of the corresponding uncrosslinked and crosslinked neat NR samples are also shown in Figure 4. The stress–strain behavior of the NR was significantly changed by the inclusion of the clay. The tensile strength of the NR distinctly was improved by the clay dispersion in both uncrosslinked and crosslinked NR, when compared with their counter parts. After gradual increase of the strain, a sharp stress increment was observed for all samples; i.e., the occurrence of stress-upturn. It is obvious that the stress-upturn of both uncrosslinked and crosslinked NR/clay nanocomposites started at lower strain than that of the neat NR. Furthermore, the tensile strength of the NR/clay nanocomposites was clearly higher than that of neat NR, and the increase of stress with applied strain in the uncrosslinked NR/clay nanocomposite was different from that of the crosslinked NR/clay one. The increase of stress for the uncrosslinked NR/clay nanocomposite was apparently larger than that of crosslinked NR/clay one. The reason why the tensile stress of the uncrosslinked NR/clay nanocomposite was higher than that of the crosslinked one will be discussed later.

WAXD Observation

Two-dimensional WAXD was performed to analyze the crystallization and orientation of the NR molecules. The 2D WAXD images coupled with their corresponding linear diffraction patterns, azimuthally integrated in the range of azimuthal angles from 80° to 100°, of the two different NR/clay nanocomposites and crosslinked neat NR at the strain of 200% are shown in Figure 5. From Figure 5, the reflection spots assigned to (200) and (120) planes for highly oriented crystalline NR was detected for the uncrosslinked and PhOH-crosslinked nanocomposites [Figure 5(a)]. The diffraction peaks corresponding to (200) and (120) planes from the NR were also observed for the uncrosslinked and PhOH-crosslinked nanocomposites [Figure 5(b)]. On the other hand, these reflection spots and diffraction peaks were not observed in the crosslinked neat NR (Figure 5) at the same strain. From the 2D WAXD analysis, it was suggested that the addition of layered silicate caused the alignment of NR chains in the stretching direction at low level of strain (<300%), leading to the formation of crystallized region in the NR matrix.

Based on the 2D WAXD image, the crystallinity (X_c) of the stretched NR could be estimated by measuring the WAXD intensity of the diffraction peaks, corresponding to the (200) and (120) planes (Figure 6), as reported by Hernandez *et al.*[28,29] The diffraction intensity in the equator direction was normalized and azimuthally integrated in the range of the azimuthal angles from 80° to 100° as shown in Figure 6. The area of the crystalline diffraction peaks assigned to the (200) and (120) planes and the area of amorphous halo were fitted by using Origin®9.1 software. The X_c was calculated using eq. (1);

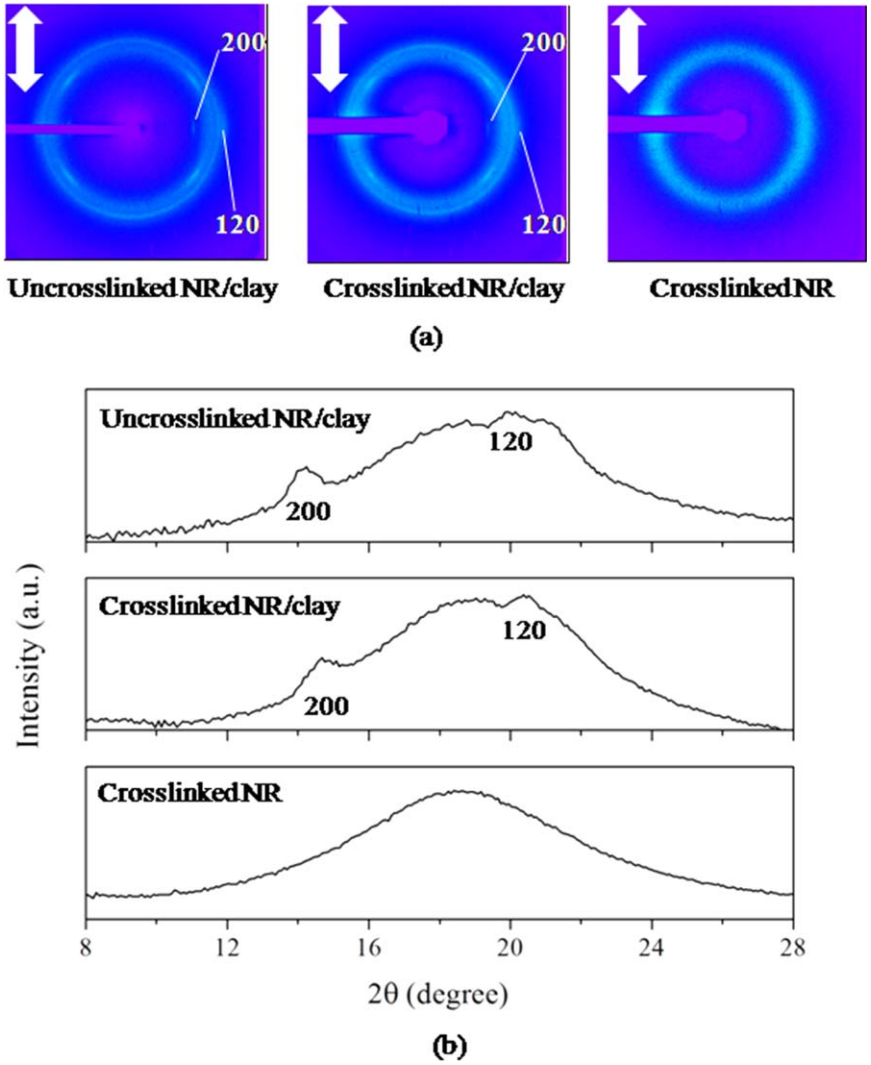

Figure 5. Coupled (a) 2D WAXD images and (b) WAXD patterns of crosslinked neat NR and NR/clay nanocomposites measured at strain of 200%. [Color figure can be viewed in the online issue, which is available at wileyonlinelibrary.com.]

$$X_c = \frac{A_c}{A_c + A_a} \times 100\ \% \quad (1)$$

where A_c is the area of crystalline diffraction peaks, corresponding to the (200) and (120) planes, and A_a is the area of the amorphous halo.

The estimated crystallinity (X_c) of the uncrosslinked and crosslinked NR/clay nanocomposites and crosslinked neat NR samples as a function of applied strain is shown in Figure 7. The crystallinity of all specimens increased with increasing strain, indicating that the crystallization of these materials was attributed to the strain-induced crystallization of the NR matrix. The crystallinity was increased in the order that crosslinked NR/clay nanocomposite > uncrosslinked NR/clay nanocomposite > cross linked neat NR. Different from the crosslinked neat NR, the NR/clay nanocomposites started to crystallize at lower strain. For example, the crystallization of the NR matrix was developed at the strain of about 100% in the uncrosslinked and crosslinked NR/clay nanocomposites, while that of the crosslinked neat NR was at about 280%. This suggested that the strain-induced crystallization of the NR could be accelerated by the incorporation of the clay, as reported by authors[17,19,20,29] for the onset of NR crystallization upon the addition of organically modified clay.

From Figure 7, it is obvious that the crystallinity of the uncrosslinked NR/clay nanocomposite began at the same strain with the crosslinked NR/clay nanocomposite, and increased with applied strain. Because the effect of the crosslink on NR crystallization of the uncrosslinked NR/clay nanocomposite could be eliminated, it is clearly explained that the crystallization of NR was caused only by the presence of clay, and was effective even at high strain. These observations indicated that the crystallization induced by the clay initiated from lower strain than the one originated from the crosslink points. More precisely, the

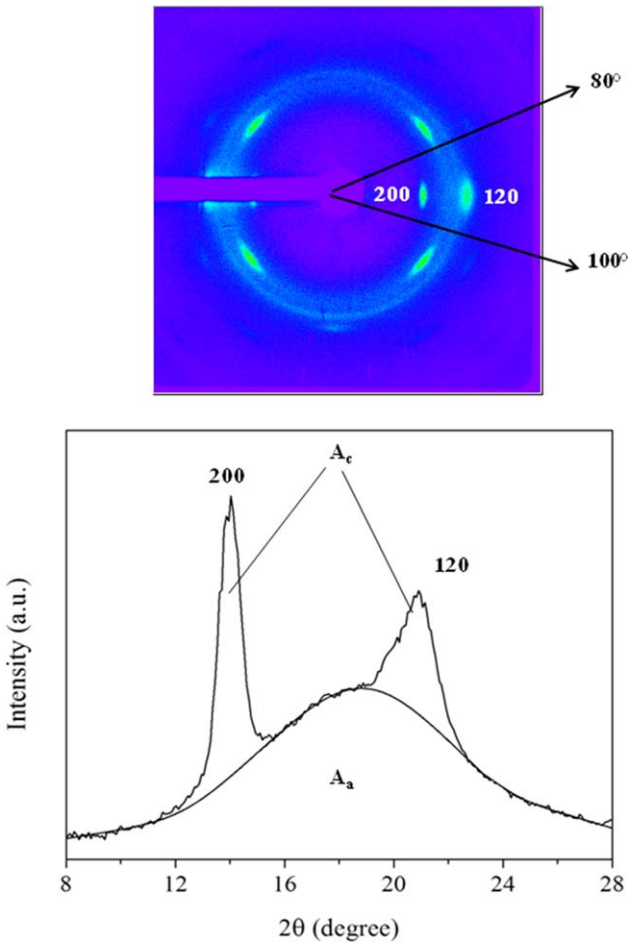

Figure 6. Typical WAXD images and WAXD profiles as a function of diffraction angle of crosslinked NR/clay nanocomposite selected at 400% strain. [Color figure can be viewed in the online issue, which is available at wileyonlinelibrary.com.]

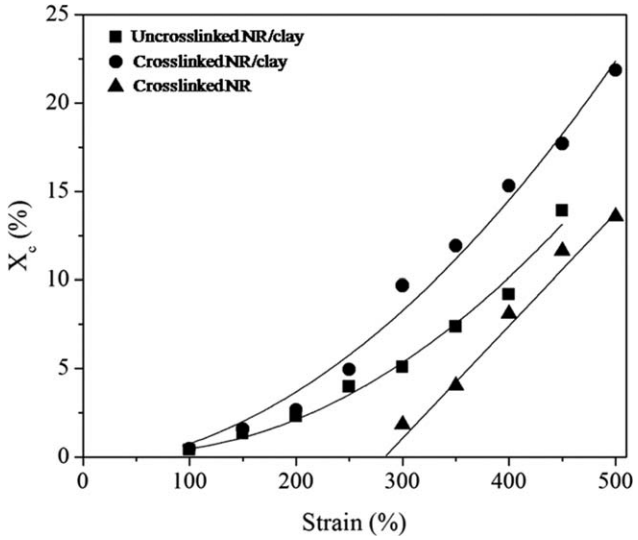

Figure 7. Change of crystallinity (X_c) as a function of strain for uncrosslinked NR/clay nanocomposite, phenolic resin-crosslinked NR/clay nanocomposite and crosslinked neat NR.

crystallization induced by the clay started at the strain of approx. 100%, whereas that related to the crosslink points started at the strain of approx. 280%. Therefore, we could presume that the great increases of tensile stress at low strain region (<300%) in the uncrosslinked and crosslinked NR/clay nanocomposites, as shown in Figure 4, were attributed to the enhancement of strain-induced crystallization by the clay.

As can be seen from Figure 7, the strain-induced crystallization of the crosslinked NR/clay nanocomposite drastically increased at the strain applied above about 300%, at which the crystallization induced from the crosslinking points just began as indicated by the crystallinity (X_c) data for the crosslinked neat NR (Figure 7). As a result, the increase of the crystallinity of the crosslinked nanocomposite became greater than that of the uncrosslinked nanocomposite at higher level of strain (>300%), although the crystallinity of these two NR/clay nanocomposites started at almost the same strain. Furthermore, the crystallinity of the PhOH-crosslinked nanocomposite was much higher than that of the crosslinked neat NR due to the contribution of NR crystallinity enhancement by the presence of clay. Similar behavior was also reported for the sulfur and peroxide crosslinked NR/clay nanocomposites.[14–20] As a result, the drastic increase of stress in the crosslinked NR/clay nanocomposite at high strain region above 300% was due to the collaborative crystallization induced by clay and conventional crosslink points, whereas the increase of the stress at low strain level (<300%) was mainly dominated by the crystallization induced by the clay as described previously. According to previous investigation,[18] with the conventional sulfur curing system, the content of unmodified nanoclay at 15 phr was used to prepare NR/clay nanocomposite. At high strain level, i.e., 400%, they found that the crystallinity index of the sulfur-crosslinked nanocomposite was about 15%, and the stress at 400% was about 2.5 MPa, which was approximately 80% greater than that of the virgin crosslinked one (~1.4 MPa). Although the crystallinity index at similar strain obtained in our study (16%) was comparable to that reported in publication,[18] but the stress at 400% of the PhOH-crosslinked nanocomposite with low addition of 5 phr unmodified clay was 3.5 MPa, which suggested the improvement level over the neat PhOH-crosslinked NR (~1.4 MPa) by about 150% (Figure 4). This indicates that the combined use of PhOH and unmodified nanoclay offers the benefit for the production of NR nanocomposite having higher level of property when compared with commonly used sulfur crosslinking system.

Figure 8 shows the orientation function (f) of the neat NR and NR/clay nanocomposites as a function of strain during stretching. The orientation function was calculated by Hermann's equation[30,31] from the azimuthal angle dependence of the WAXD intensity (Figure 9). From Figure 8, it is seen that the values of f were negative, and their magnitude increased with increasing strain, indicating that the degree of orientation in the NR crystallites increased with increasing strain. The change of f value for the NR/clay nanocomposites was obtained at lower

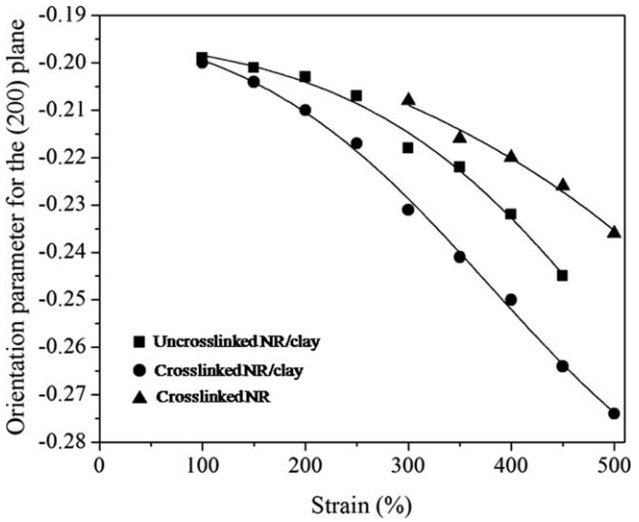

Figure 8. Change of orientation parameters (f) as a function of strain for uncrosslinked NR/clay nanocomposite, phenolic resin crosslinked NR/clay nanocomposite and crosslinked neat NR.

strain, comparing with the crosslinked neat NR. As shown in Figure 8, the change of the f value for the crosslinked nanocomposite was also higher than that of the uncrosslinked NR/clay nanocomposite, nevertheless the change of f value was observed at almost the same strain. These results corresponded to the increase of the crystallinity (X_c) with increasing strain as already shown in Figure 7. That is, the increase of the crystallinity with higher strain was associated with the increase of the orientation of NR chains. Thus, the increase of NR crystalline for the crosslinked NR/clay nanocomposite was mainly explained as follows; the orientation of the NR chains was increased in the presence of clay, and the increase of the crystallinity at high strain region above 300% was caused by the increase of NR chain orientation by collaborative effects of clay and crosslinking points.

SAXS Analysis

It is known that the clay stacks and single clay platelets in the NR matrix could be rotated and aligned by stretching, resulting in clay orientation.[32] To understand the orientation of clay during the stretching, 2D SAXS measurement was performed and the 2D SAXS images of the uncrosslinked and crosslinked NR/clay nanocomposites at various strains are shown in Figure 10. The result of the crosslinked neat NR was also included. From Figure 10, the circular pattern was seen in all specimens at the strain of 0%. The pattern of the PhOH-crosslinked neat NR was almost unchanged by stretching. In contrast, the pattern of the uncrosslinked and crosslinked NR/clay nanocomposite changed from circular one to ellipsoidal one during stretching. Therefore, it is clear that the change of the pattern for the uncrosslinked and crosslinked nanocomposites was influenced by the rotation of the dispersed clay. Generally, the circular pattern in the NR/clay nanocomposite was seen when the clay was randomly oriented at the strain of 0%. Because the shape of clay is plate-like structure, therefore the ellipsoidal pattern appeared as a result of the clay orientation and the dimension of ellipsoidal shaped pattern in the perpendicular direction to the stretching one became greater with increasing the degree of

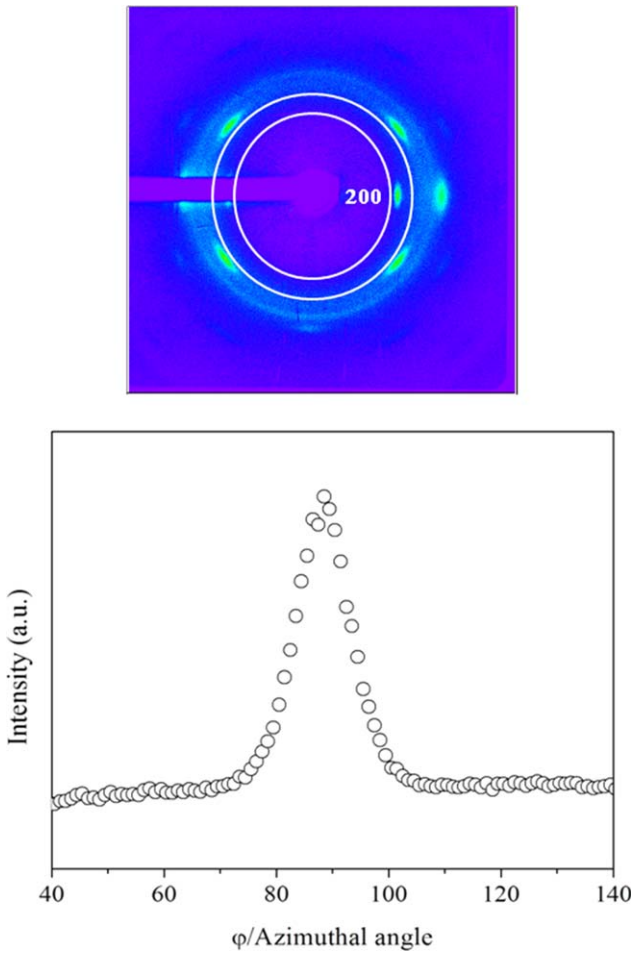

Figure 9. Typical WAXD image and WAXD profile as a function of azimuthal angle of crosslinked NR/clay nanocomposite selected at 400% strain. [Color figure can be viewed in the online issue, which is available at wileyonlinelibrary.com.]

orientation. The aspect ratio of the ellipsoidal pattern defined as L/D, where L is maximum dimension in perpendicular direction to the stretching and D is maximum dimension in parallel direction to the stretching, was increased with the increase of the orientation of the clay. Hence, the orientation of the clay could be determined by the change of aspect ratio of the 2D SAXS image.

The aspect ratios of the 2D SAXS images of the various NR samples as a function of strain are shown in Figure 11. The aspect ratios of the uncrosslinked and crosslinked NR/clay nanocomposites increased in response to the level of strain applied. On the contrary, no significant change of the aspect ratio was observed for the simply crosslinked NR. These results suggested that the rotation of the clay was taken placed at small strain (100%) and then the clay was aligned along stretching direction according with increasing strain. As described previously, we demonstrated that the crystallinity (X_c) (Figure 7) and the degree of orientation (f) (Figure 8) of the NR matrix in the NR/clay nanocomposites were developed at the low strain of 100%. Judging from the result of crystallization and orientation of NR, it is considered that the clay was also rotated and

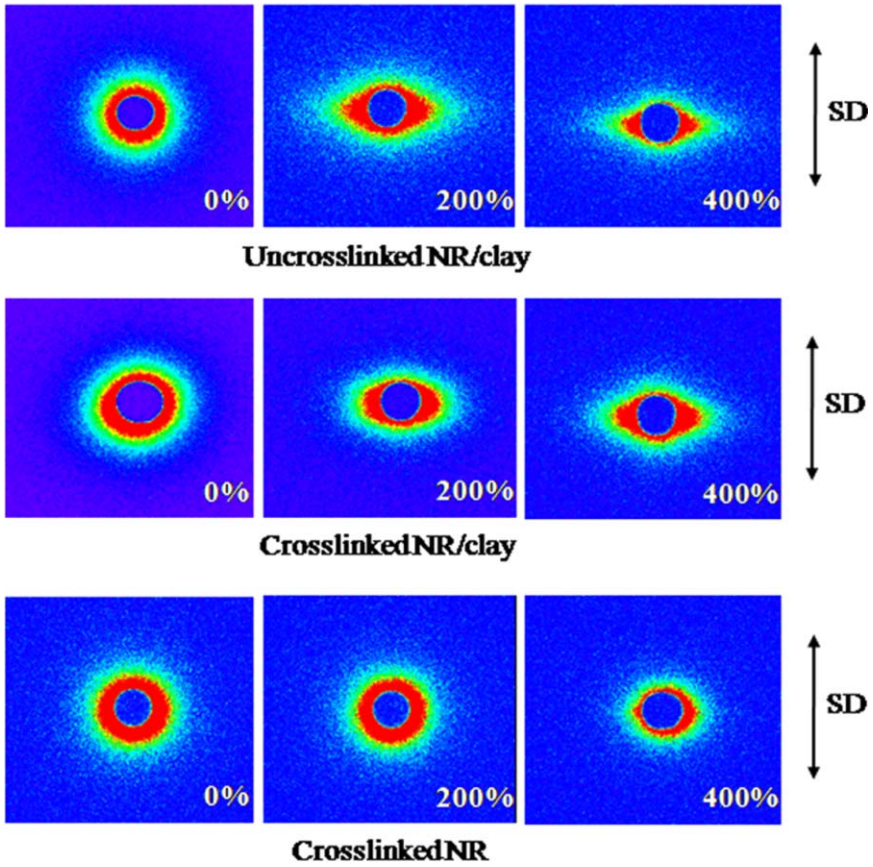

Figure 10. Two-dimensional SAXS images of crosslinked neat NR and NR/clay nanocomposites measured at various strains (SD = stretching direction). [Color figure can be viewed in the online issue, which is available at wileyonlinelibrary.com.]

oriented in the stretching direction even at low strain level of 100%. Thus, the strain-induced crystallization for the NR/clay nanocomposites observed at the low strain of 100% strain was associated with the orientation of the clay.

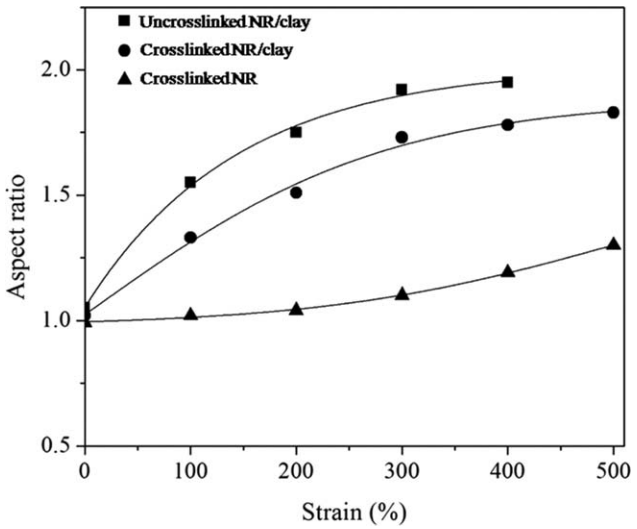

Figure 11. Change of aspect ratios as a function of strain for uncrosslinked NR/clay nanocomposite, phenolic resin-crosslinked NR/clay nanocomposite and crosslinked neat NR.

It is interesting to note that the aspect ratio of the uncrosslinked NR/clay nanocomposite was higher than that of the crosslinked one, although the crystallinity and orientation parameter of the NR in the uncrosslinked NR/clay nanocomposite were smaller than those of the crosslinked nanocomposite (Figures 7 and 8). This might be attributed to the prevention of the clay orientation by existence of the crosslinked network of NR chains. Referring back to the results shown in Figure 4, the tensile stress of the uncrosslinked NR/clay nanocomposite was higher when the crosslinked one was compared, especially at lower strain region (<300%). During tensile test, the sample was uniaxially deformed, the clay particles rotated and became aligned with their axes running parallel to the stretching direction, this would lead to better stress transfer ability. Apparently, the thickness of single clay platelet is about 1 nm[11] and the average thickness of clay tactoids dispersed in the uncrosslinked NR nanocomposite was less than that of the crosslinked NR/clay nanocomposite (Figure 2). This means that the number of platelets stacked within the clay tactoids was also less for the uncrosslinked sample. Increasing number of platelets in the intercalated clay tactoids resulted in decreasing tensile modulus of clay in the direction parallel to platelet plane.[33] Thus, the combination of both preferred alignment and greater tensile modulus of anisotropic clay surely led to more reinforcement efficiency for the uncrosslinked NR/clay nanocomposite. Moreover, the tensile stress of the uncrosslinked NR/clay

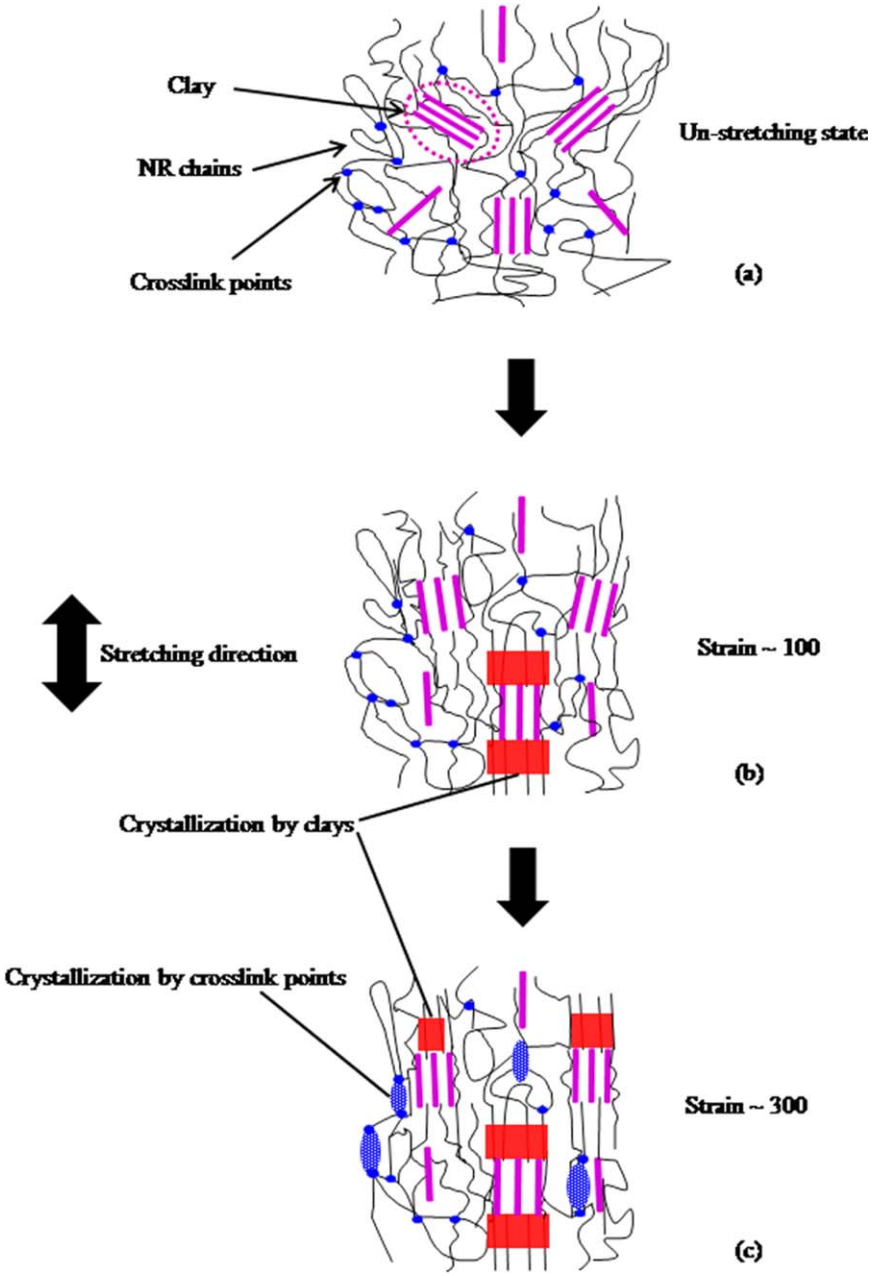

Figure 12. Proposed model for strain-induced crystallization mechanism of phenolic resin-crosslinked NR/clay nanocomposite during stretching. [Color figure can be viewed in the online issue, which is available at wileyonlinelibrary.com.]

nanocomposite continued to increase at the strain above 300%, even though the orientation of the clay almost completed and the crosslinking points did not exist. This phenomenon suggested that the crystallization of NR induced from the clay was also effective after completing the orientation of the clay. As the strain-induced crystallization by the clay continuously occurred, the increase of the tensile strength for the crosslinked NR/clay nanocomposite at high strain region above 300% was much greater than those of the uncrosslinked NR/clay nanocomposite and crosslinked neat NR. This could be explained with the collaborative crystallization of NR by the dispersion of clay and crosslink points as described in the previous section.

From these results, the schematic illustration was proposed for the strain-induced crystallization in the crosslinked NR/clay nanocomposite, as shown in Figure 12. In this scheme, the nanometer-sized tactoids were dispersed in the crosslinked NR/clay nanocomposite, and the NR matrix was possibly connected to the clay tactoids through intercalation of NR chain and strong adhesion *via* specific interaction between PhOH functionalized NR and clay [Figure 12(a)]. Study on interaction between clay, NR, and PhOH-crosslinking agent is being performed and the research results will be reported in future publication. During stretching the nanocomposites, the plate-like shaped clay was orientated and aligned along the stretching direction. The

crystallization of the NR matrix was then induced due to the stress concentration at the surface of the clay, and the crystallinity (as well as the degree of NR crystallite orientation) became increased in association with the orientation of the clay [Figure 12(b)]. Subsequently, the NR chains were rearranged and crystallized at higher strain about 300% [Figure 12(c)]. Finally, the crystallinity of the NR matrix was steeply increased due to the collaborative crystallization of NR enhanced by dispersed clay and crosslink points at strain above 300%. Thus, the significant increase of tensile strength was obtained.

CONCLUSION

NR/unmodified clay nanocomposites consisting of intercalated clay structure and thin tactoids of nanometer scale were successfully prepared and were crosslinked with phenolic resin (PhOH). The effect of clay addition on the crystallization and molecular orientation of NR was studied. In the presence of clay, the tensile strength significantly increased for both the uncrosslinked and crosslinked NR/clay nanocomposites owing to the acceleration of strain-induced crystallization of NR. At low strain, the crystallization of crosslinked NR containing clay was mainly attributed to the clay dispersion. However, at high strain, the crystallization was considerably enhanced by the clay and the crosslink points. Owing to the collaborative crystallization enhancement by the clay addition and crosslinking points, the tensile strength of the crosslinked NR/clay nanocompoiste was much greater than those of the uncrosslinked nanocomposite and the crosslinked neat NR, particularly at high strain region. A mechanistic model for the strain-induced crystallization and orientational evolution of a network structure of phenolic resin-crosslinked NR/clay nanocomposite was proposed. The study on the changes of the clay dispersion during vulcanization with PhOH and the interaction between clay, NR and PhOH is being performed and the research results will be reported in the near future.

ACKNOWLEDGMENTS

We gratefully acknowledge financial support from the Thailand Research Fund (TRF) through the Royal Golden Jubilee Ph.D. Program (Grant No. PHD/0052/2554). A scholarship supported by Prince of Songkla Graduate Studies Grant, Prince of Songkla University to the first author is gratefully acknowledged.

REFERENCES

1. Roberts, A. D. Natural Rubber Science and Technology; Oxford University Press: New York, **1988**.
2. Kohjiya, S.; Ikeda, Y. Chemistry, Manufacture and Applications of Natural Rubber; Woodhead Publishing: United Kingdom, **2014**.
3. Ciullo, P. A.; Hewitt, N. The Rubber Formulary; Noyes Publications: New York, **1999**.
4. Toki, S.; Sics, I.; Ran, S.; Liu, L.; Hsiao, B. S.; Murakami, S.; Senoo, K.; Kohjiya, S. *Macromolecules* **2002**, *35*, 6578.
5. Murakami, S.; Senoo, K.; Toki, S.; Kohjiya, S. *Polymer* **2002**, *43*, 2117.
6. Toki, S.; Hsiao, B. S. *Macromolecules* **2003**, *36*, 5915.
7. Tosaka, M.; Murakami, S.; Poompradub, S.; Kohjiya, S.; Ikeda, Y.; Toki, S.; Sics, I.; Hsiao, B. S. *Macromolecules* **2004**, *37*, 3299.
8. Arroyo, M.; Lopez-Manchado, M. A.; Herrero, B. *Polymer* **2003**, *44*, 2447.
9. Messersmith, P. B.; Giannelis, E. P. *J. Polym. Sci. Part A: Polym. Chem.* **1995**, *33*, 1047.
10. Giannelis, E. P. *Appl. Organomet. Chem.* **1998**, *12*, 675.
11. Thomas, S.; Stephen, R. Rubber Nanocomposites: Preparation, Properties and Applications; Wiley: Singapore, **2010**.
12. Lopattananon, N.; Tanglakwaraskul, S.; Kaesaman, A.; Seadan, M.; Sakai, T. *Int. Polym. Proc.* **2014**, *29*, 332.
13. Joly, S.; Garnaud, G.; Ollitrault, R.; Bokobza, L. *Chem. Mater.* **2002**, *14*, 4202.
14. Qu, L.; Huang, G.; Zhang, P.; Nie, Y.; Weng, G.; Wu, J. *Polym. Int.* **2010**, *59*, 1397.
15. Nie, Y.; Qu, L.; Huang, G.; Wang, B.; Weng, G.; Wu, J. *Polym. Adv. Technol.* **2012**, *23*, 85.
16. Nie, Y.; Huang, G.; Qu, L.; Wang, X.; Weng, G.; Wu, J. *Polymer* **2011**, *52*, 3234.
17. Carretero-Gonzalez, J.; Verdejo, R.; Toki, S.; Hsiao, B. S.; Giannelis, E. P.; Lopez-Manchado, M. A. *Macromolecules* **2008**, *41*, 2295.
18. Carretero-Gonzalez, J.; Retsos, H.; Verdejo, R.; Toki, S.; Hsiao, B. S.; Giannelis, E. P.; Lopez-Manchado, M. A. *Macromolecules* **2008**, *41*, 6763.
19. Nie, Y.; Qu, L.; Huang, G.; Wang, X.; Weng, G.; Wu, J. *J. Appl. Polym. Sci.* **2014**, *131*, 40324.
20. Qu, L.; Huang, G.; Liu, Z.; Zhang, P.; Weng, G.; Nie, Y. *Acta Mater.* **2009**, *57*, 5053.
21. Shell, J.; Wang, T.; Tokita, N.; Chung, B. *Rubber World* **2000**, *221*, 40.
22. He, S.-J.; Wang, Y.-Q.; Wu, Y.-P.; Wu, X.-H.; Lu, Y.-L.; Zhange, L.-Q. *Plast. Rubber Compos.* **2010**, *39*, 33.
23. Wu, Y.-P.; Wang, Y.-Q.; Zhang, H.-F.; Wang, Y.-Z.; Yu, D.-S.; Zhang, L.-Q.; Yang, J. *Compos. Sci. Technol.* **2005**, *65*, 1195.
24. Osaka, N.; Kato, M.; Saito, H. *J. Appl. Polym. Sci.* **2013**, *129*, 3396.
25. Lattimer, R. P.; Kinsey, R. A.; Layer, R. W. *Rubber Chem. Technol.* **1989**, *62*, 107.
26. Choi, S.-S.; Cho, G. *J. Appl. Polym. Sci.* **1998**, *68*, 1811.
27. Duin, M.; Souphanthong, A. *Rubber Chem. Technol.* **1995**, *68*, 717.
28. Hernandez, M.; Lopez-Manchado, M. A.; Sanz, A.; Nogales, A.; Ezquerra, T. A. *Macromolecules* **2011**, *44*, 6574.
29. Hernandez, M.; Sanz, A.; Nogales, A.; Ezquerra, T. A.; Lopez-Manchado, M. A. *Macromolecules* **2013**, *46*, 3176.
30. Garcia-Gutierrez, M. C.; Hernandez, J. J.; Nogales, A.; Panine, P.; Rueda, D. R.; Ezquerra, T. A. *Macromolecules* **2008**, *41*, 844.
31. Roe, R.-J. Methods of X-Ray and Neutron Scattering in Polymer Science; Oxford University Press: New York, **2000**.
32. Shah, D.; Maiti, P.; Jiang, D. D.; Batt, C. A.; Giannelis, E. P. *Adv. Mater.* **2005**, *17*, 525.
33. Fornes, T. D.; Paul, D. R. *Polymer* **2003**, *44*, 4993.